MR Brain Image Segmentation Using an Improved Kernel Fuzzy Local Information C-Means Based Wavelet, Particle Swarm Optimization (PSO) Initialization and Outlier Rejection with Level Set Methods

Abdenour Mekhmoukh and Karim Mokrani
Laboratoire de Technologie Industrielle et de l'Information, Université de Bejaia, Algeria

Abstract: *This paper, presents a new image segmentation method based on Wavelets, Particle Swarm Optimization (PSO) and outlier rejection caused by the membership function of the Kernel Fuzzy Local Information C-Means (KFLICM) algorithm combined with level set is proposed. The segmentation of Magnetic Resonance (MR) images plays an important role in the computer-aided diagnosis and clinical research, but the traditional approach which is the Fuzzy C-Means (FCM) clustering algorithm is sensitive to the outlier and does not integrate the spatial information in its membership function. Thus the algorithm is very sensitive to noise and in-homogeneities in the image, moreover, it depends on cluster centers initialization. A novel approach, named improved IKFLICMOR is presented to improve the outlier rejection and reduce the noise sensitivity of conventional FCM clustering algorithm. To get the first image segmentation, the traditional FCM is applied to low-resolution image after wavelet decomposition. In general, the FCM algorithm chooses the initial cluster centers randomly, but the use of PSO algorithm gives us a good result for these centers. Our algorithm is also completed by adding into the standard FCM algorithm the spatial neighborhood information. These a priori are used in the cost function to be optimized. The resulting fuzzy clustering is used as the initial level set function. The results confirm the effectiveness of the IKFLICMOR associated with level set for MR image segmentation.*

Keywords: *Image segmentation, outlier rejection, FCM, PSO, spatial fuzzy clustering, wavelet transform, level set methods.*

Received May 24, 2015; accepted March 9, 2016

1. Introduction

The Magnetic Resonance Imaging (MRI) is a very developed area [17, 18]. It can help us to diagnose various diseases. Several classification techniques are used for brain MR image segmentation among which thresholding [24] edge detection [4], region growing [20] and clustering [7] are the most well-known ones. Noise affects these techniques and thus, leads to incorrect boundaries detection, under and over-segmentation, and difficulties in threshold selection for the edge image. These image segmentation methods, have led to region growing algorithms. These methods are the extension of thresholding by considering the homogeneity and connectivity criteria. Region growing algorithms [7] can robustly identify only well-defined regions. Knowing that the above-mentioned techniques are generally used for relatively simple structures, clustering methods are applied for complex data. In clustering we use similar characteristics for grouping data. Fuzzy C-Means (FCM) algorithms [11, 15, 19, 27] are the typical, well known method used in image segmentation. Many modifications of the FCM algorithm have been proposed to alleviate the effects of noise, like Noisy Clustering (NC) [8], robust fuzzy local information C-Means Clustering [13], Robust Fuzzy C-Means (RFCM) algorithm [16] and Outlier Rejection Fuzzy C-Means (ORFCM) [23].

This paper is organized as follows. Section 2 is a background concept of the FCM and its limitations. The implementation of the proposed algorithm is presented in section 3. In section 4 we present the performance of the proposed algorithm and comparisons with other algorithms. Finally, the conclusion is presented in section 5.

2. Background

2.1. Fuzzy C-Means Algorithm (FCM)

The The FCM clustering algorithm was first introduced by Dunn [9] and then extended by Trelea [25]. Let $X=\{xi\}$ an image, $i=\{1,2,\ldots n\}$ where x_i are the pixels of an image X and n is the total number of pixels. The FCM algorithm minimizes the objective function [19]:

$$J_{FCM} = \sum_{i=1}^{c}\sum_{k=1}^{n} \mu_{ik}^{m} d^{2}(x_k, V_i) \quad (1)$$

U represents the membership function matrix, d the distance metric between the element x_j and the cluster center V_i and m the degree of fuzziness (m>1).

The membership function U is the heart of the FCM where the membership degrees are given by

$$\mu_{ik} = \frac{1}{\sum_{j=1}^{c}\left(\frac{d_{ik}}{d_{jk}}\right)^{\frac{2}{m-1}}} \quad (2)$$

Where μ_{ik} is the membership degree of x_i and V_i represent the cluster:

$$V_i = \frac{\sum_{i=1}^{n}\mu_{ik}^{m}x_k}{\sum_{k=1}^{n}\mu_{ik}^{m}} \quad (3)$$

2.2. Kernel Fuzzy C-Means (KFCM) Algorithm

In KFCM, the original Euclidian distance is replaced by the following expression [28]:

$$d(x,y) = \|\Phi(x) - \Phi(y)\| \quad (4)$$

$$d(x,y) = \sqrt{K(x,x) - 2K(x,y) + K(y,y)} \quad (5)$$

- ϕ is a nonlinear function and the Gaussian kernel used is :

$$K(x,y) = \exp\left(-\frac{\|x-y\|^2}{\sigma^2}\right) \quad (6)$$

The KFCM objective function is:

$$J_{KFCM} = \sum_{i=1}^{c}\sum_{k=1}^{n}\mu_{ik}^{m}\|\Phi(x_k) - \Phi(V_i)\|^2 \quad (7)$$

$$J_{KFCM} = 2\sum_{i=1}^{c}\sum_{k=1}^{n}\mu_{ik}^{m}(1 - K(x_k, V_i)) \quad (8)$$

The membership degrees become

$$\mu_{ik} = \frac{(1-K(x_k,V_i))^{\frac{-1}{m-1}}}{\sum_{j=1}^{c}(1-K(x_k,V_j))^{\frac{-1}{m-1}}} \quad (9)$$

And the cluster centers are now:

$$V_i = \frac{\sum_{k=1}^{n}\mu_{ik}^{m}K(x_k,V_i)x_k}{\sum_{k=1}^{n}\mu_{ik}^{m}K(x_k,V_i)} \quad (10)$$

2.3. Fuzzy Local Information C-Means (FLICM) Algorithm

Krinidis and Chatzis [13] propose the following object function:

$$J_{FLICM} = \sum_{i=1}^{N}\sum_{k=1}^{c}\mu_{ki}^{m}d^2(x_i,V_k) + G_{ki} \quad (11)$$

The term G is given as:

$$G_{ki} = \sum_{\substack{j\in N_i \\ i\neq j}}\frac{1}{d_{ij}+1}(1-\mu_{kj})^m\|x_j - V_k\|^2 \quad (12)$$

Where: d_{ij} is the spatial Euclidian distance between pixels i and j

$\|x_j\text{-}V_k\|^2$Is a Euclidian distance between object x_j and cluster center V_k .

The membership of FLICM is updated as:

$$\mu_{ki} = \frac{1}{\sum_{j}^{c}\left(\frac{\|x_i - V_k\|^2 + G_{ki}}{\|x_i - V_j\|^2 + G_{ji}}\right)^{\frac{2}{m-1}}} \quad (13)$$

And the cluster centers are now:

$$V_k = \frac{\sum_{i=1}^{N}\mu_{ki}^{m}x_i}{\sum_{i=1}^{N}\mu_{ki}^{m}} \quad (14)$$

3. Proposed Algorithm

3.1. Improved Kernel Fuzzy Local Information C-Means algorithm and Outlier Rejection (IKFLICMOR)

In this section, we propose to modify the algorithm IKFLICMOR by considering the fuzzy partition matrix, pixels spatial information and the initialization cluster centers. The proposed algorithm is described in these steps:

1. Wavelet Transform to get the initialized labels.
2. Replacing Euclidian distance with Mahalanobis.
3. Cluster centers initialization using PSO algorithm.
4. Improve the membership function of the FLICM algorithm by considering outlier rejection and Gaussian kernel.
5. Using Level set to finalize the segmentation.

3.1.1. Wavelet Transform

Wavelet analysis is a technique of multi-resolution analysis and time -scale analysis. In initial segmentation, the advantage of the high-frequency coefficients is not considered. Shi *et al*. [22] suggested that the best initial segmentation results can be obtained by applying the FCM to the low-frequency image of the coarse scale. Using the wavelet analysis, the low-frequency image of the coarse-scale has a small amount of data, but also has the global information and most of the energy of image. We apply conventional FCM to low-frequency image of the coarse-scale in order to obtain the initial segmentation result and each pixel obtains only a label.

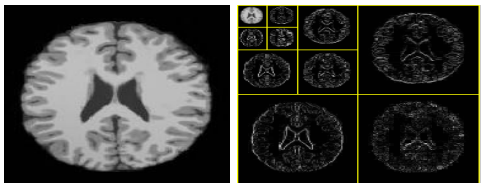

a) Original image. b) DWT decomposition at level 3.

Figure 1. Image DWT decomposition.

From the reconstructed image, a label is assigned for each pixel. The similarity of two pixels increases if the two pixels' labels are same, and their distance is reduced:

$$\beta_{ij} = \begin{cases} t & x_i \text{ and } v_j \text{ are of the same labels} \\ 1 & x_i \text{ and } v_j \text{ are of the different labels} \end{cases} \quad (15)$$

The distance between two pixels is:

$$d_{ij} = \left\| \beta^{\alpha}{}_{ij} (y_j - y_i) \right\|^2 \quad (16)$$

Where B_{ij} is the similarity between x_{ij} and the cluster center V_j, $y_i$and y_j are the pixels' vector value. α is described later in section outlier rejection and Gaussian kernel.

3.1.2. Mahalanobis Distance

The Mahalanobis distance is defined as:

$$\left\| x_j - V_k \right\|^2 = (x_j - V_k)^T S_k (x_j - V_k) \quad (17)$$

$$S_k = \left| \sum_k \right|^{\frac{1}{P}} \sum_k^{-1} \quad (18)$$

p=1: the dimension of the problem.

3.1.3. Membership Function and Cluster Centers Initialization

For the initialization step of our algorithm, a Swarm Particles Optimization is used to have better initial clusters centers. Kennedy and Eberhart [12] and Trelea [25] proposed a PSO method which is a population based stochastic optimization algorithm, inspired by fish schooling and bird flocking.

The following Equations govern the evolution of the swarm:

$$V^{(k+1)} = wV^{(k)} + c_1 rand_1 (pbest^{(k)} - X^{(k)}) + c_2 rand_2 (gbest^{(k)} - X^{(k)}) \quad (19)$$

$$X^{(k+1)} = V^{(k)} + X^{(k)} \quad (20)$$

X, *V*, *pbest*, *gbest*, *rand*1, *rand*2 and k are respectively the position of the particle, velocity of the particle, the best position of the particle, the global best position of the swarm, random values between 0 and 1 and the iteration number.

Table 1. Parameters values used in the PSO initialization.

Parameters	Values
c1=c2	1.70
W	[0.4 0.9]
Eps	10^{-6}
$nb_{maxiter}$	300
n_{erp}	10
Number of particles	12

The values of the parameters of Equation (19) used are given in Table 1. The values of *c*1 and *c*2 are those recommended by Trelea [25]. The inertia weight *w* is adapted over the PSO iterations; this parameter varies linearly from 0.9 to 0.4 for $nb_{maxiter}$ iterations. The high starting value of this parameter promotes diversification (exploration). The decrease of this value favors intensification (exploitation). This scenario, often used in metaheuristics, allows optimizing the results by regulating the balance between exploration and exploitation of the search space.

For the stopping condition, we used two criteria:

1. The non-significant improvements of the objective function after n_{erp} iterations.
2. The maximum number of iterations $nb_{maxiter}$.

$$\begin{aligned} &\forall k \in [0, nb_{\max iter}], \forall n \in [k, k + nb_{erp}] \\ &|J(n+1) - J(n)| < \text{Eps} \end{aligned} \quad (21)$$

3.1.4. Outlier Rejection and Gaussian Kernel

Let $X=\{xi\}$ an image, $i=\{1,2,...n\}$ where x_i are the pixels of an image *X* and *n* represents the total number of pixels. As shown in section 2, the FCM or FLICM uses a metric distance which is very sensitive to the outliers. The membership function of the FLICM algorithm is modified by considering first the Kernel function and then outlier rejection.

The mathematical model of the IKFLICMOR is:

$$\min J_{IKFLICMOR} = \sum_{i=1}^{N} \sum_{k=1}^{c} \mu_{ki}^m \alpha^{(1-K(x_i,V_k))} + G_{ki} \quad (22)$$

The membership function of the FLICM algorithm is modified by replacing the original distance term in Equation (11).

$$\mu_{ki} = \frac{1}{\sum_{j=1}^{c} \left(\frac{\alpha^{(1-K(x_i,V_k))} + G_{ki}}{\alpha^{(1-K(x_i,V_j))} + G_{ji}} \right)^{\frac{2}{m-1}}} \quad (23)$$

$$V_k = \frac{\sum_{i=1}^{N} \mu_{ki}^m K(x_i, V_k) x_i}{\sum_{i=1}^{N} \mu_{ki}^m K(x_i, V_k)} \quad (24)$$

The factor *G* is modified as:

$$G_{ki} = \sum_{\substack{j \in N_i \\ i \neq j}} \frac{1}{d_{ij} + 1} (1 - \mu_{kj})^m \alpha^{(1-K(x_i,V_j))} \quad (25)$$

Where:

$$K(x_i, V_k) = \exp\left(-\frac{\left\| x_i - V_k \right\|^2}{\sigma^2}\right) \quad (26)$$

σ is the bandwidth . A pixel *i* is assigned to class c:

$$C_i = \arg\left\{ \max\left\{ \mu_{kj} \right\} \right\}, \quad k = 1,2,3 \cdots, c \quad (27)$$

The role of the exponent variable α is to limit the partial distribution of the points among the 2 neighbouring clusters rather than to all of the clusters. The exponent variable α is defined as:

$$\alpha = \frac{(\text{Range of intensity in an image}) + 1}{\text{Maximum range of intensity} + 1} + 1 \quad (28)$$

For an 8bit grayscale image, Equation (28) is given:

$$\alpha = \frac{(X_{max} - X_{min}) + 1}{256} + 1 \quad (29)$$

Where X_{max} is the maximum intensity in an image and X_{min} is the minimum intensity in an image. The exponent variable α is between 1 and 2. In an image if it contains a large range of intensity, the exponent variable α is close to 2 and it could reduce the partial distribution of the points between 2 adjacent clusters. Unlike if the image contains a small range of intensity, the exponent variable α is close to 1 and the points among the adjacent clusters only. In this example Figure 2, the data are generated in the intensity range of 1 to 120 and portioned in 3 clusters, c_1 , c_2 , and c_3 by FCM algorithm which groups the data into 3 regions, c_1 , c_2 , and c_3 , with membership functions u_1(red), u_2(green), and u_3(blue), respectively. In the range of 0 to 60, the membership $u_1$isassigned to the outliers for cluster $c_1$and these outliers could produce insufficient effects by pulling away the center from their optimum level. This decreases the variance intercluster and increases the intracluster.

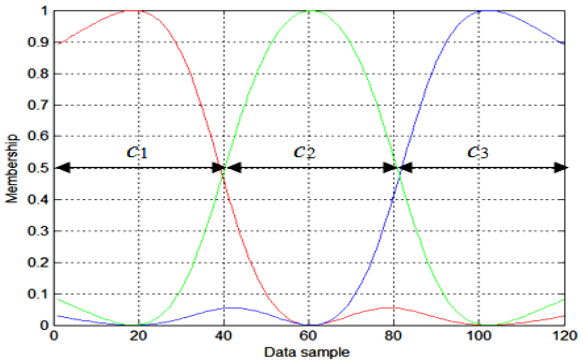

a) FCM.

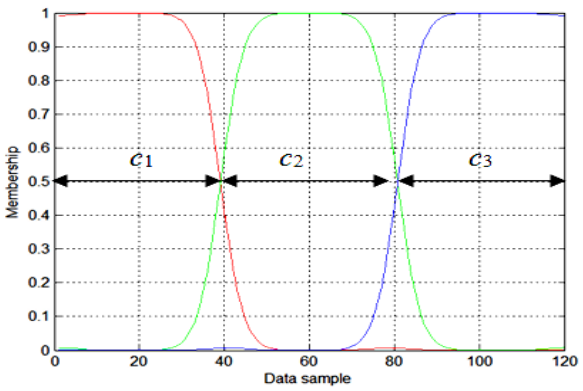

b) IKELICMOR.

Figure 2. Membership functions for data of intensity range 1 to 120.

By cons in example (Figure 2-b), we can see that the outliers have approximately a zero membership value.

3.1.5. Level Set Segmentation

We use level set method to finalize the segmentation after obtained a good value of special fuzzy clustering by IKFLICMOR. Segmenting images by means of active contours is a well known approach [6, 14], but instead of a parametric characterization of active contours, level set methods embed them into a time dependent PDE function $\psi(t,x,y)$. It is then possible to approximate the evolution of the active contours implicitly by tracking the zero level set $\Gamma(t)$.

$$\begin{cases} \psi(t,x,y) < 0 & (x, y) \text{ is inside } \Gamma(t) \\ \psi(t,x,y) = 0 & (x, y) \text{ is at } \Gamma(t) \\ \psi(t,x,y) > 0 & (x, y) \text{ is inside } \Gamma(t) \end{cases} \quad (30)$$

Γ may be comprised of a single or a series of zero isocontours. It can be easily determined by checking the values of the level set function, which adapt to topological changes of the implicit interface Γ. The evolution ending is determined by:

$$\begin{cases} \frac{\partial \psi}{\partial t} + F|\nabla \psi| = 0 \\ \psi(0,x,y) = \psi_0(x,y) \end{cases} \quad (31)$$

Where $|\nabla \psi|$ is the normal direction, $\psi_0(x, y)$is the initial contour and F represents the comprehensive forces.

The evolving force F has to be regularized by an edge indication function g in order to stop the level set evolution near the optimal solution

$$g = \frac{1}{1 + |\nabla (G_\sigma * I)|^2} \quad (32)$$

Where $G_\sigma * I$ is the convolution between a smoothing Gaussian kernel G_σ and the image I. and ∇ denotes the operation for an image gradient. Level set segmentation is formulated as [14]

$$\frac{\partial \psi}{\partial t} = g|\nabla \psi| \left(div\left(\frac{\nabla \psi}{|\nabla \psi|} \right) + \nu \right) \quad (33)$$

Where $div\left(\frac{\nabla \psi}{|\nabla \psi|} \right)$ approximates mean curvature κ and v is a customable balloon force.

A fast level set algorithm was proposed by [15]:

$$\frac{\partial \psi}{\partial t} = \mu \zeta(\psi) + \xi(g, \psi) \quad (34)$$

Where $\zeta(\psi)$ is the penalty momentum of ψ and $\xi(g,\psi)$ is an image gradient information

$$\xi(g,\psi) = \lambda \delta(\psi) + div\left(g \frac{\nabla \psi}{|\nabla \psi|} \right) + \nu\, g\, \delta(\psi) \quad (35)$$

Where δ (ψ)is Dirac function. v, μand λ parameters to control the level set .The initial level set function ψ_0 is obtained from IKFLICMOR fuzzy clustering.

Here the summarize steps of our algorithm

(Algorithm 3 and Figure 3):

Algorithm 3: IKFLICMOR

- *Step 1: Initialize (c: number of class, m>1: degree of fuzziness,ε: stopping criterion.)*
- *Step 2: Initialize ($U^{(0)}$ and $V^{(0)}$) using Algorithm 2.*
- *Step 3:t=1*
- *Step 4: calculate($U^{(t)}$) using :*

$$\mu_{ki}^{(t)} = \frac{1}{\sum_{j=1}^{c}\left(\frac{\alpha^{(1-K(x_i, V_k^{(t-1)}))} + G_{ki}}{\alpha^{(1-K(x_i, V_j^{(t-1)}))} + G_{ji}}\right)^{\frac{2}{m-1}}}$$

- *Step 5 : Update($V^{(t)}$) using :*

$$V^{(t)}{}_k = \frac{\sum_{i=1}^{N} \mu_{ki}^{(t-1)m} K(x_i, V_k) x_i}{\sum_{i=1}^{N} \mu_{ki}^{(t-1)m} K(x_i, V_k)}$$

- *Step 6: If* $|U^t - U^{t-1}| < \varepsilon$ *stop, else t=t+1 and return to step.4*

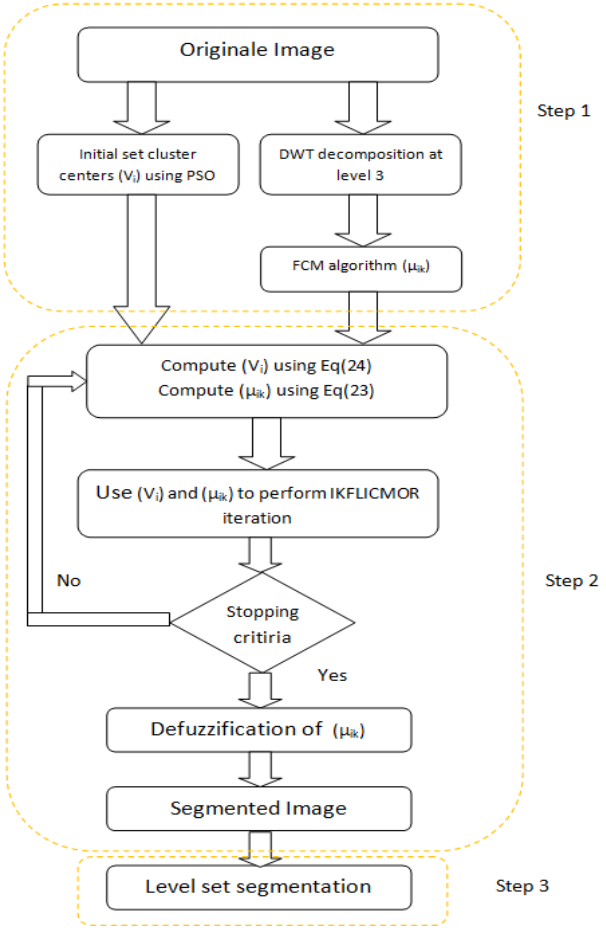

Figure 3. The process of the proposed method.

4. Experiments and Result Analysis

In this section, the results of the IKFLICMOR algorithm are presented and compared to those of standard FCM algorithm and other algorithms. First, we used a synthetic image in which noise is localized in its center. This problem is often found in MRI images where intensity in-homogeneities, can be simulated as local noise.

a) Synthetic images: We use a synthetic image (Figure 4) (181x140) with five gray levels and different type of (salt and pepper, Gaussian and Uniform).

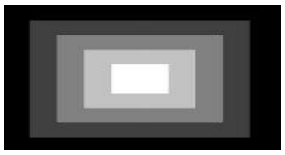

Figure 4 .Synthetic image.

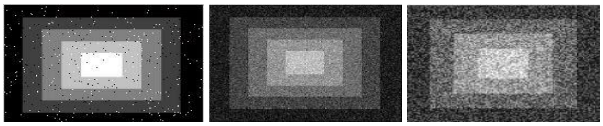

a) salt and pepper. b) Gaussian. c) Uniform.

Figure 5. Noised image.

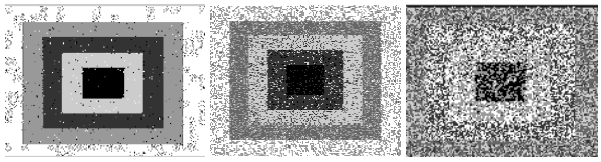

a) salt and pepper. b) Gaussian. c) Uniform.

Figure 6. FCM segmentation results.

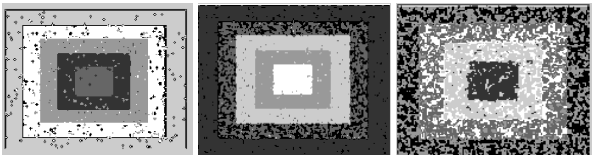

a) salt and pepper. b) Gaussian. c) Uniform.

Figure 7. FCM_S1 segmentation results.

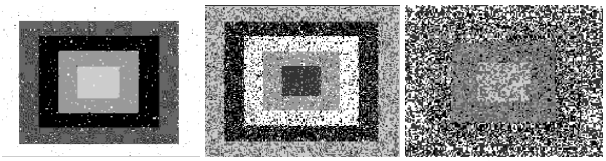

a) salt & pepper. b) Gaussian. c) Uniform.

Figure 8. FLICM segmentation results.

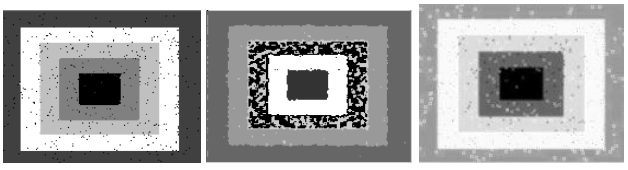

a) salt & pepper. b) Gaussian. c) Uniform.

Figure 9. IKFLICMOR segmentation results.

The comparison of FCM, FCM_S1, FLICM and IKFLICMOR results are given in Figure 5 to 9 respectively. Although the FCM algorithm can segment the image, many noises still exist in both regions. The traditional FCM was unable to correctly classify the images but our IKFLICMOR approach can get better result than FLICM algorithm and outperforms the conventional FCM.

b) Simulated medical images: Healthy brain tissue can be classified into three tissues. These are White

Matter (WM), Cerebro-Spinal Fluid (CSF) and Grey Matter (GM) [5]. The second type example is a simulated MR brain image from the Brain Web Simulated Brain Database [3]. This database was chosen since it is very frequently as a benchmark for the scientific community. For experimentation, we have chosen three noise levels (0%, 5% and 9%). For a better segmentation, the parameters of the algorithm, namely the values of m and the number of classes C, and finally the vectors form representing the image pixels are defined. We set the number of class (c = 4) which are the three brain tissue (cerebrospinal fluid, white matter, grey matter) and background. The choice of the vector form is made of the pixel grey levels.

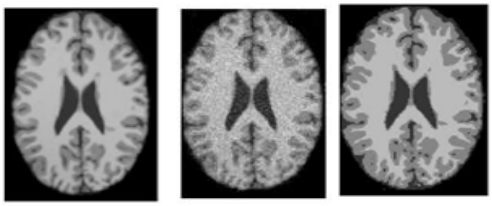

a) Original image. b) FCM. c) IKFLICMOR.

Figure 10. Results for an axial slice T1 with 5% of noise.

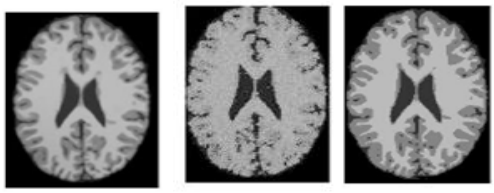

a) Original image. b) FCM. c) IKFLICMOR.

Figure 11. Results for an axial slice T1 with 9% of noise.

Figures 10 and 11 give us a comparison of segmentation results between FCM and IKFLICMOR. From these results, the traditional FCM is not suitable to classify the images but IKFLICMOR gives good results despite the fact that the images are affected by noise. Because of its ability to cope with noise IKFLICMOR gives better results than FCM. Obviously, with an increase of the noise level, the segmentation result of FCM degrades rapidly.

To evaluate the performance of clustering, we use two functions, and partition entropy V_{pe} [2] and partition coefficient V_{pc} [1] .They are defined as follows:

$$Vpe = \frac{1}{n}\sum_{i=1}^{c}\sum_{j=1}^{n}\mu_{ij}^{2} \tag{36}$$

$$Vpc = \frac{1}{n}\sum_{i=1}^{c}\sum_{j=1}^{n}\mu_{ij}\log(\mu_{ij}) \tag{37}$$

The validity function is used to compare between FCM, FCM_S1, FLICM and IKFLICMOR. A best clustering is obtained if the value V_{pe} is minimal or V_{pc} is maximal. Another validity functions based on the feature structure is used [23, 26]:

$$Vxb = \frac{\sum_{i=1}^{c}\sum_{j=1}^{n}\mu_{ij}^{2}\left\|x_j - v_i\right\|^2}{n\left(\min_{i\neq k}\left\{\left\|x_k - v_i\right\|^2\right\}\right)} \tag{38}$$

Table 2. Results for the synthetic image.

Validity function / Noise level	V_{pc}			V_{pe}			V_{xb}		
	1%	5%	9%	1%	5%	9%	1%	5%	9%
FCM	0.8831	0.8723	0.8457	0.2312	0.3122	0.4125	0.0623	0.0687	0.0856
FCM_S1	0.9322	0.9145	0.8612	0.1913	0.2157	0.3023	0.0517	0.0697	0.0933
FLICM	0.9612	0.9518	0.9289	0.1002	0.1538	0.1844	0.0525	0.0497	0.0301
IKFLICMOR	**0.9896**	**0.9734**	**0.9675**	**0.0474**	**0.0723**	**0.0912**	**0.0329**	**0.0462**	**0.0476**

Table 3. Results for simulated MRI image.

Validity function / Noise level	V_{pc}			V_{pe}			V_{xb}		
	1%	5%	9%	1%	5%	9%	1%	5%	9%
FCM	0.8814	0.8520	0.8293	0.2468	0.2891	0.2949	0.0561	0.0676	0.0848
FCM_S1	0.9233	0.9037	0.8859	0.1789	0.1922	0.2831	0.0492	0.0590	0.0731
FLICM	0.9620	0.9420	0.9224	0.1063	0.1465	0.1967	0.0251	0.0463	0.0576
IKFLICMOR	**0.9827**	**0.9731**	**0.9615**	**0.0438**	**0.0725**	**0.0873**	**0.0293**	**0.0317**	**0.0436**

c) Tissues Extraction: Brain tissue extraction for MRI image with 9% noise, using FCM, FLICM, and IKFLICMOR, are given in Figures 12 and 13 respectively

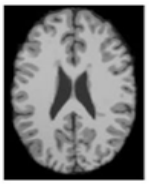

a) Original image.

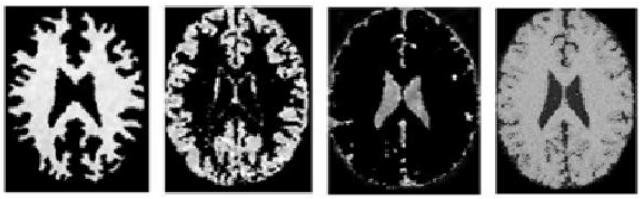

b) WM. c) GM. d) CSF. e) Global.

Figure 12. FCM results for simulated MRI image with 9% of noise.

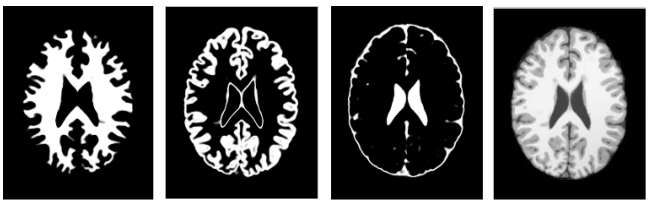

a) WM. b) GM. c) CSF. d) Global.

Figure 13. IKFLICMOR results for simulated MRI image with 9% of noise.

For a quantitative evaluation of the results, a pixel based evaluation approach is used. A comparison is made between pixels of the resulting image (R_t) and

the ground truth (R_g). The following measures are used; Dice index, Jaccard index, True Positive Fraction (TPF), False Negative Fraction (FNF), False Positive Fraction (FPF) and True Negative Fraction (TNF). [10, 21] As the basis of measurements: for the Dice, Jaccard, TPF and TNF approaches, whenever the results are higher, the performances are better. Meanwhile for the rest of the basis of measurements which are *FNF* and *FPF*, the lower results indicate better performances.

$$Dice = \frac{2|R_t \cap R_g|}{|R_t| + |R_g|} \quad ; \quad Jaccard = \frac{R_t \cap R_g}{R_t \cup R_g} \tag{39}$$

$$TPF = \frac{R_t \cap R_g}{R_g} ; Jaccard = \frac{R_t \cap R_g}{R_t \cup R_g}$$
$$FPF = \frac{R_t - R_g}{R_g} ; TNF = 1 - \frac{R_t - R_g}{R_g} \tag{40}$$

Table 4. Results of WM and GM using evaluation measures (Dice, Jaccard and FNF).

Tissues Index	WM			GM		
	Dice	*Jaccard*	*FNF*	*Dice*	*Jaccard*	*FNF*
FCM	0.8671	0.7613	0.2160	0.8588	0.7526	0.2275
FCM_S1	0.9035	0.7747	0.1046	0.8857	0.7921	0.1527
FLICM	0.9532	0.9048	0.0922	0.9558	0.9028	0.0145
IKFLICMOR	**0.9763**	**0.9559**	**0.0012**	**0.9735**	**0.9547**	**0.0023**

From Table 4, we can say that the proposed approached gives good results using the various criteria.

d) Real medical images: The first experimentation is done on real medical images Figure 14 that containing two cancerous region

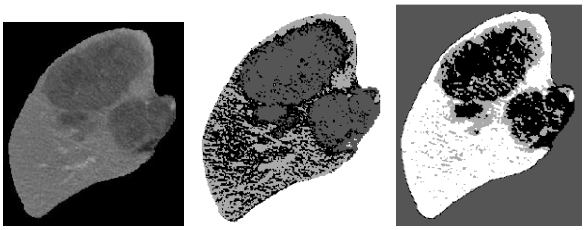

a) Original image. b) FCM. c) FCM_S1.

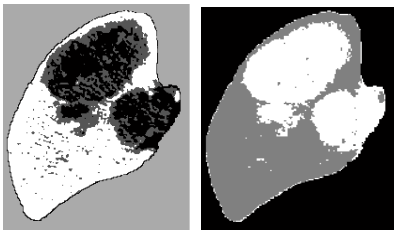

d) FLICM. e) IKFLICMOR.

Figure 14. Segmentation results.

e) Real MR Brain Images: The second experimentation is done on real brain MR images Figure 15 provided from the Internet Brain Segmentation Repository (IBSR).

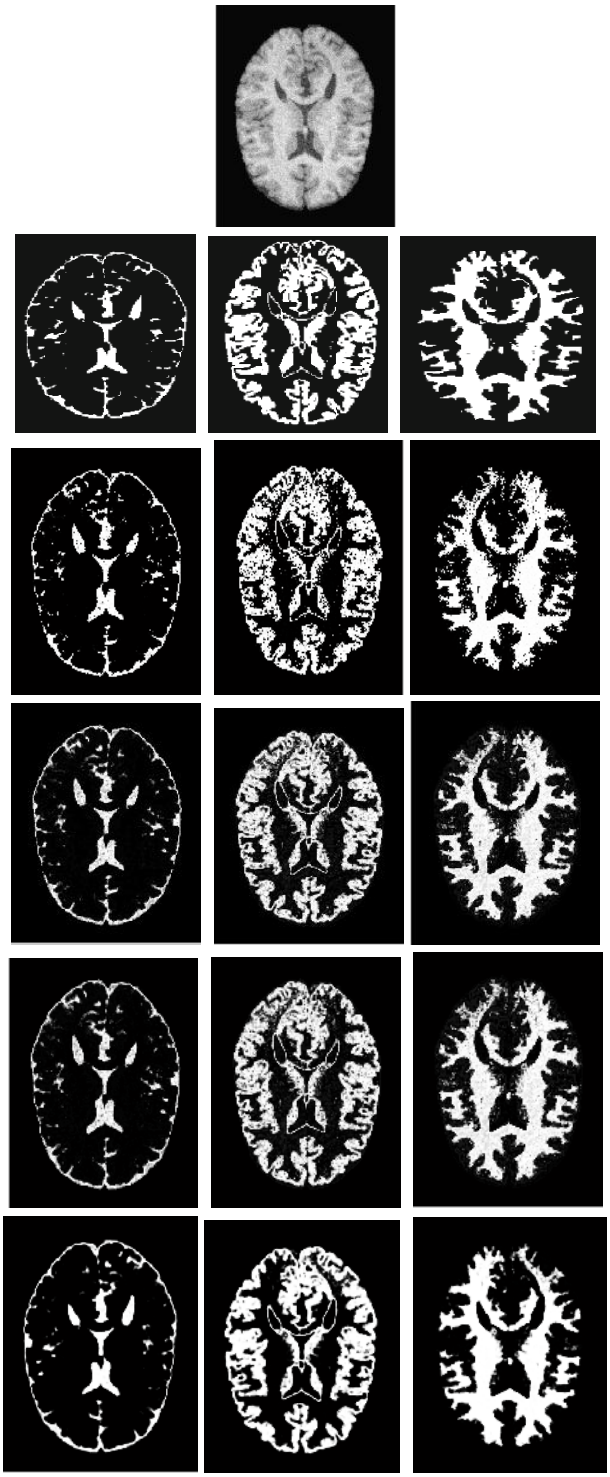

Figure 15. First row: original image, from second to 6th row respectively: FCM, FCM_S1, FLICM and IKFLICMOR segmentation results.

f) Real images: furthermore, we test the algorithm on real images Figure 16.

Figure 16. First column: original images, second columns: IKFLICMOR segmentation results.

g) Level set Segmentation: The objective of the third step of our algorithm is to initialize level set parameters using special fuzzy clustering obtained by IKFLICMOR.

Table 5. Used parameters in step 3.

Parameters	Designation	Values
μ	Coefficient of penalty term	0,1
υ	Artificial balloon force	1,5
λ	Coefficient of contour length	5
T	Maximum iteration of level set evolution	2800

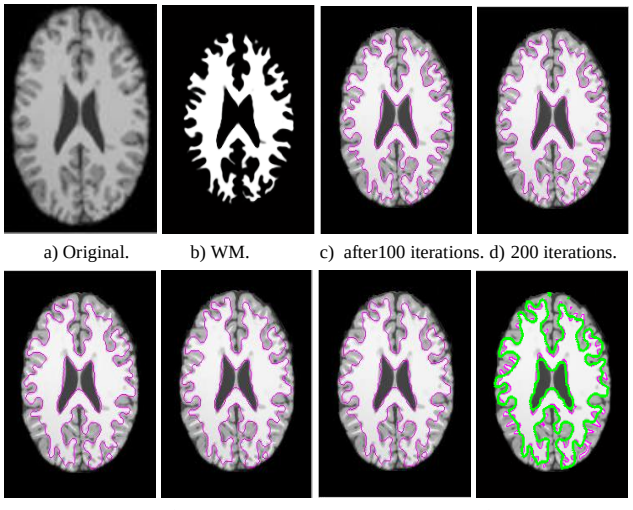

a) Original. b) WM. c) after100 iterations. d) 200 iterations.

e) 400 iterations. f) 800 iterations. g) 1600 iterations. h) final segmentation after 2000 iterations.

Figure 17. Level set segmentation of MRI cerebral tissues (WM).

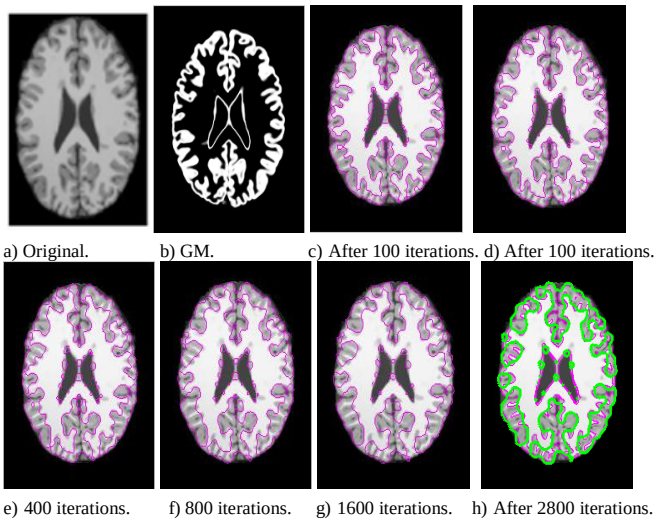

a) Original. b) GM. c) After 100 iterations. d) After 100 iterations.

e) 400 iterations. f) 800 iterations. g) 1600 iterations. h) After 2800 iterations.

Figure 18. Level set segmentation of MRI cerebral tissues (GM).

Figures 17, 18, and 19 present the results obtained after several iterations with level set algorithm.

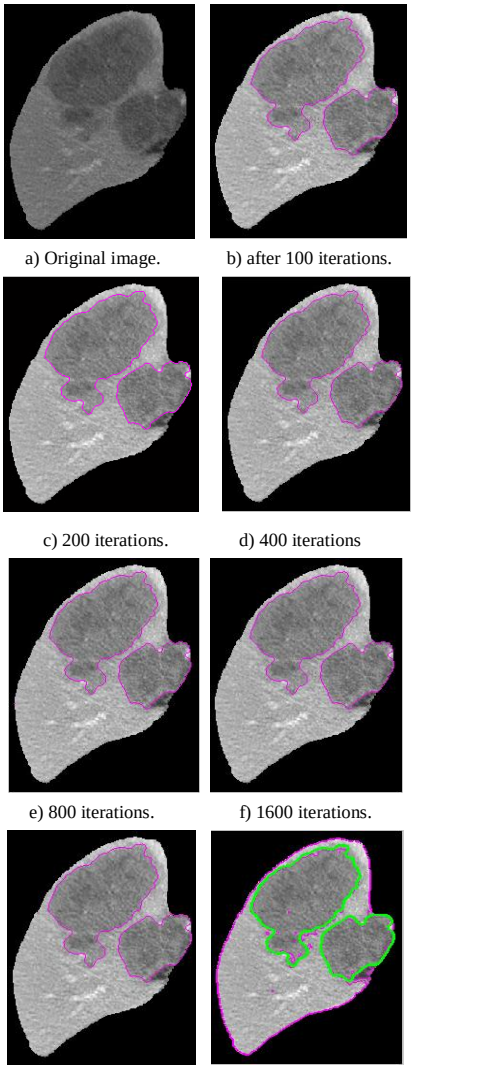

a) Original image. b) after 100 iterations.

c) 200 iterations. d) 400 iterations

e) 800 iterations. f) 1600 iterations.

g) 2000 iterations. h) segmentation after 2800 iterations (Green)

Figure 19. Level set segmentation of cancerous tissues.

5. Conclusions

In this paper, we have presented a novel FLICM algorithm where we have incorporated the spatial neighborhood information in the original FLICM algorithm, and PSO algorithm for cluster centers initialization and less sensitive to the outlier. It is tested on different images, such as synthetic and MR images. We have compared the performance of FCM, FCM_S1, FLICM and IKFLICMOR algorithms. The results show that the algorithm is well suited to the identification of classes and it shows a significant improvement concerning the robustness to noise compared to FCM, FCM_S1 and FLICM algorithms. A good results obtained with IKFLICMOR, lead to a fine segmentation and the extraction of the various tissues GM, WM and CSF using the level set method.

Finally, it is noteworthy to take in consideration the integration of other constraints on the spatial pixels arrangement and combine several classification algorithms working in cooperation in order to overcome the problems encountered by the use of a single algorithm.

References

[1] Bezdek J., "Mathematical Models for Systematic and Taxonomy," *in Proceedings of 8th International Conference on Numerical Taxonomy*, San Franscisco, pp. 143-166, 1975.

[2] Bezdek J., *Pattern Recognition with Fuzzy Objective Function Algorithms*, Plenum Press, 1981.

[3] Brain Web: Simulated Brain Database, McConnell Brain Imaging Centre, Montreal Neurological Institute McGill, Last Visited, 2014.

[4] Canny J., "A Computational Approach to Edge Detection," *IEEE Transactions on Pattern Analysis and Machine Intelligence*, vol. PAMI-8 no. 6, pp. 679-698, 1986.

[5] Chen S. and Zhang D., "Robust Image Segmentation Using FCM with Spatial Constraints Based on New Kernel-Induced Distance Measure," *IEEE Transactions on Systems, Man, and Cybernetics*, vol. 34, no. 4, pp. 1907-1916, 2004.

[6] Chuang K., Tzeng H., Chen S., Wu J., and Chen T., "Fuzzy C-means Clustering with Spatial Information for Image Segmentation," *Computerized Medical Imaging and Graphics*, vol. 30, no. 1, pp. 9-15, 2006.

[7] Clarke L., Velthuizen R., Camacho M., Heine J., Vaidyanathan M., Hall L., Thatcher R., and Silbiger M., "MRI Segmentation: Methods and Applications," *Magnetic Resonance Imaging*, vol. 13, no. 3, pp. 343-368, 1995.

[8] Dave R., "Characterization and Detection of Noise in Clustering," *Pattern Recognition Letters*, vol. 12, no. 11, pp. 657-664, 1991.

[9] Dunn J., "A Fuzzy Relative of the ISODATA Process and its use in Detecting Compact Well-Separated Clusters," *Journal of Cybernetics*, vol. 3, no. 3, pp. 32-57, 1973.

[10] Elnakib A., Gimel'farb G., Suri J., and El-Baz A., *Medical Image Segmentation: a Brief Survey: Multi Modality State-of-the-Art Medical Image Segmentation and Registration Methodologies*, Springer, pp. 1-39, 2011.

[11] Kalti K. and Mahjoub M., "Image Segmentation by Gaussian Mixture Models and Modified FCM Algorithm," *The International Arab Journal of Information Technologie*, vol. 11, no. 1, pp. 11-18, 2014.

[12] Kennedy J. and Eberhart R., "Particle Swarm Optimization," *in Proceedings of the 6th International Symposium on Micro Machine and Human Science*, Nagoya, pp. 1-9, 1995.

[13] Krinidis S. and Chatzis V., "A Robust Fuzzy Local Information C-means Clustering Algorithm," *IEEE Transactions on Image Processing*, vol. 19, no. 5, pp. 1328-1337, 2010.

[14] Li B., Chui C., Chang S., and Ong S., "Integrating Spatial Fuzzy Clustering with Level Set Methods for Automated Medical Image Segmentation," *Computers in Biology and Medicine*, vol. 41, no. 1, pp. 1-10, 2011.

[15] Li C., Goldgof D., and Hall L., "Knowledge-Based Classification and Tissue Labeling of MR Images of Human Brain," *IEEE Transactions on Medical Imaging*, vol. 12, no. 4, pp. 740-750, 1993.

[16] Maji P. and Paul S., "Rough-Fuzzy Clustering for Grouping Functionally Similar Genes from Microarray Data," *IEEE/ACM Transactions on Computational Biology and Bioinformatics*, vol. 10, no. 2, pp. 286-299, 2013.

[17] Pham D. and Prince J., "Adaptive Fuzzy Segmentation of Magnetic Resonance Images," *IEEE Transactions on Medical Imaging*, vol. 18, no. 9, pp. 737-752, 1999.

[18] Pham D., Xu C., and Prince J., "Current Methods in Medical Image Segmentation," *Annual Review of Biomedical Engineering*, vol. 2, no. 1, pp. 315-337, 2000.

[19] Pham D., "Spatial Models for Fuzzy Clustering," *Computer Vision and Image Understanding*, vol. 84, no. 2, pp. 285-297, 2001.

[20] Pohle R. and Toennies K., "Segmentation of Medical Images Using Adaptive Region Growing," *in Proceedings of SPIE-The International Society for Optical Engineering*, San Diego, 2001.

[21] Prasad M., Divakar T., Rao B., and Raju N., "Unsupervised Image Thresholding using Fuzzy

Measures," *International Journal of Computer Applications*, vol. 27, no. 2, pp. 32-41, 2011.
[22] Shi Z., Liu Y., and Li Q., "Medical Image Segmentation Based on FCM and Wavelets," *in Proceedings of Intelligence Science and Big Data Engineering*, Beijing, pp. 279-286, 2013.
[23] Siddiqui F., Isa N., and Yahya A., "Outlier Rejection Fuzzy C-means Algorithm for Image Segmentation," *Turkish Journal of Electrical Engineering and Computer Sciences*, vol. 21, no. 6, pp. 1801-1819, 2013.
[24] Suzuki H. and Toriwaki J., "Automatic Segmentation of Head MRI Images by Knowledge Guided Thresholding," *Computerized Medical Imaging and Graphics*, vol. 15, no. 4, pp. 233-240, 1991.
[25] Trelea I., "The Particle Swarm Optimization Algorithm: Convergence Analysis and Parameter Selection," *Information Processing Letters*, vol. 85, no. 6, pp. 317-325, 2003.
[26] Xie X. and Beni G., "A Validity Measure for Fuzzy Clustering," *IEEE Transactions on Pattern Analysis and Machine Intelligence*, vol. 13, no. 8, pp. 841-847, 1991.
[27] Zanaty E. and Aljahdalia S., "Improved Fuzzy Algorithms for Automatic Magnetic Resonance Image Segmentation," *The International Arab Journal of Information Technologie*, vol. 7, no. 3, pp. 271-279, 2010.
[28] Zhang D. and Chen S., "A Novel Kernelized Fuzzy C-means Algorithm with Application in Medical Image Segmentation," *Artificial Intelligence in Medicine*, vol. 32, no. 1, pp. 37-50, 2004.

Abdenour Mekhmoukh Received his engineering degree in electronics in 2004 from University of Bejaia, Algeria, Magister in Automatics and signal processing in 2008 and Doctorate in 2016. He is currently a senior lecturer in the Electrical Engineering department in the University of Bejaia, Algeria. His research interests include signal, image processing.

Karim Mokrani Received his engineering degree in electronics in 1982 from University of Algers, Algeria, an MSEE and Ph.D. degrees in electrical engineering in 1985 and 1988 respectively from Southern Methodist University, Dallas, USA. He is currently professor in the Electrical Engineering department in the University of Bejaia, Algeria. His research interests include signal, image processing and digital video processing.